

Article

Study on Detecting Method of Internal Defects by Laser Ultrasonics in Lap Joint Welding of Galvanized Steel Sheet and Finite Element Analysis of Its Detectability

Norimitsu Okuyama ¹, Kazufumi Nomura ^{1,*}, Tomokazu Sano ¹ , Keiji Kadota ², Seiya Nitta ², Tetsuo Era ² and Satoru Asai ²

¹ Graduate School of Engineering, Osaka University, Osaka 565-0871, Japan;

n.okuyama@mapse.eng.osaka-u.ac.jp (N.O.); sano@mapse.eng.osaka-u.ac.jp (T.S.)

² DAIHEN Welding and Joining Research Alliance Laboratories, JWRI Osaka University, Osaka 567-0047, Japan; era@daihen.co.jp (T.E.); asai@mapse.eng.osaka-u.ac.jp (S.A.)

* Correspondence: nomura@mapse.eng.osaka-u.ac.jp; Tel.: +81-6-6879-4494

Abstract: Blowholes caused by vaporization of the galvanized layer are a problem with galvanized steel sheets, which use lap joint welding. The laser ultrasonic method is the possible solution to realize the desirable 100% inspection instead of the conventional sampling inspection. We have previously proposed a method to detect blowholes by capturing the reduction in ultrasonic intensity when it passes through internal defects through signal processing. However, there was a problem that the detection indicator devised varied. In this study, we investigated the causes and trends of detectability using finite element analysis. To efficiently calculate the results obtained by scanning measurement, we proposed and established a method to reproduce the results by taking the results from static measurements, which were shifted in the direction of the weld line little by little. As a result, it was found that one of the reasons for the detection indicator variation with scanning by the lasers is the three-dimensional positional relationship between the blowhole and the scanning measurement line. In addition, it was possible to propose the performance required for the ultrasonic generation laser such as the traveling speed and the repetition frequency by back-calculating the spatial resolution from the rate of detection needed.

Keywords: laser ultrasonics; internal defect; finite element method; non-destructive inspection



Citation: Okuyama, N.; Nomura, K.; Sano, T.; Kadota, K.; Nitta, S.; Era, T.; Asai, S. Study on Detecting Method of Internal Defects by Laser Ultrasonics in Lap Joint Welding of Galvanized Steel Sheet and Finite Element Analysis of Its Detectability. *Appl. Sci.* **2023**, *13*, 11515. <https://doi.org/10.3390/app132011515>

Academic Editor: Jacek Tomków

Received: 8 September 2023

Revised: 27 September 2023

Accepted: 9 October 2023

Published: 20 October 2023



Copyright: © 2023 by the authors. Licensee MDPI, Basel, Switzerland. This article is an open access article distributed under the terms and conditions of the Creative Commons Attribution (CC BY) license (<https://creativecommons.org/licenses/by/4.0/>).

1. Introduction

There have been many cases of destruction originating from welds [1]. Therefore, further improvement in the reliability of welded part is required. At present, the quality evaluation of welds is performed after welding, in other words, post-processing, and when defects are detected, repair welding is performed again as necessary. For thin-plate welded joints, sampling inspection is generally performed because total inspection is not practical with conventional inspection methods, which include a destructive inspection. However, it is impossible to determine the presence or absence of defects in all welded parts by sample inspection. Therefore, according to the sampling inspection results, repairs are made or discarded on a lot-by-lot, resulting in huge costs. Thus, assurance by total inspection is required. For this purpose, a non-destructive inspection method applicable in situ, which can accommodate relatively high-speed welding for thin plates, is needed. In particular, galvanized steel sheets are in high demand in many fields such as for automobile body panels because of their superior corrosion resistance, lightweight, and economic efficiency. However, galvanized steel sheets are prone to pore defects called blowholes in the overlapped area in lap joint welding [2]. This is due to the evaporation of the galvanized layer during welding, and the gases generated penetrate the molten pool and remain there. Although it is possible to reduce the occurrence of blowholes by creating gaps in the overlap

area, it is difficult to control the gaps. There is a great need for the quality assurance of galvanized steel sheets. In-process monitoring for weld quality including the presence or absence of weld defects in parallel with the welding process is very effective in meeting these requirements for welding galvanized steel sheets with lap joint welding.

In-process monitoring requires establishing a measurement method that can be applied in high-temperature and high-noise environments during welding. However, conventional non-destructive inspection methods such as ultrasonic testing (UT) require a transducer to contact the measurement target to acquire internal information, making it difficult to apply and automate such methods in high-temperature environments. Thus, a non-contact method is desirable. Several methods can be used for this purpose such as the X-ray method [3], an ultrasonic method using buffer rods [4], electromagnetic ultrasonic method [5], airborne ultrasonic method [6], and laser ultrasonic method [7]. Among them, the laser ultrasonic method, in which ultrasonic waves are excited by irradiating a pulsed laser onto the target surface, and the ultrasonic waves propagating inside or on the surface and reflected at various interfaces are received by a laser interferometer, is suitable for in-process monitoring due to the following features. (1) Using a laser as a probe allows non-contact measurement with the object. (2) The point-to-point measurement by lasers makes it applicable to narrow areas. (3) Optical mirrors and mechanical stages can scan the lasers, and information on ultrasonic propagation at multiple points can easily be obtained. With these features, it has been used for defect measurement [8,9] including the detection of internal defects [10–13]. In addition, there have been many research reports on plate thickness measurement [14] and material evaluation [15,16].

On the other hand, there are no reports of the in-process detection of internal defects in thin-plate welds. Most of the experiments on thin-plate components are limited to specimens with simplified geometry, and there are only a few experiments on parts with complex geometry such as weld beads and weld reinforcement. However, if an in-process monitoring technique using the laser ultrasonic method can be established for thin-plate welded components, reliable quality assurance by total inspection can be realized.

Based on the above, we aimed to establish a detection method using laser ultrasonics that could be applied to the in-process measurement, targeting blowholes that occur in the lap joint welding of thin galvanized steel sheets. In our previous study, Nomura et al. reported a proposal for the detection method [17,18], and the details are described in Section 2. However, this detection method has a problem in that the derived detection indicator varies due to the three-dimensional relationship between the blowhole geometry and the measurement line by traveling along the welding line.

Therefore, this study aimed to clarify the causes and trends of detectability using simulations based on the finite element method. To efficiently calculate the results obtained during the traveling measurement, we proposed a method to extract the data from the static measurement and reproduce the dynamic measurement by shifts in the direction of the weld line little by little. The proposed method can be used for a wide range of studies when attempting to detect 3D defects using traveling measurement, where the advantages of non-contact inspection, as typified by laser ultrasonics, are utilized, so it is general and shows common findings for various traveling measurement systems.

2. Method and Experimental Results of Blowhole Detection in Thin Sheet Welds Using Laser Ultrasonic Techniques

This section describes our previously proposed method for detecting blowholes in the lap joint welds of thin sheets of galvanized steel using laser ultrasonics.

2.1. Theory of Detection Method

Figure 1 shows a schematic diagram of a thin-plate lap weld with blowholes in the cross-section and the generation and detection points of the laser ultrasonic. Ultrasonic waves excited on the surface of the bead reflect off the back of the lower plate and reach the surface of the lower plate. Its signal strength attenuates when it passes through an inter-

nal blowhole. The proposed method detects defects by capturing this attenuation [17,18]. Specifically, a B-scope (2D data of ultrasonic waveforms with the coordinates of the generation point on the horizontal axis and the ultrasonic propagation time on the vertical axis) was created for a single cross-sectional area. The B-scope was with multiple generation points on the bead by the pulsed laser and a single detection point on the lower plate surface by the laser interferometer. Focusing on the relevant signal area, a defect detection indicator representing attenuation was calculated, and the presence or absence of a defect was determined according to its value. The detailed results are described in the following sections.

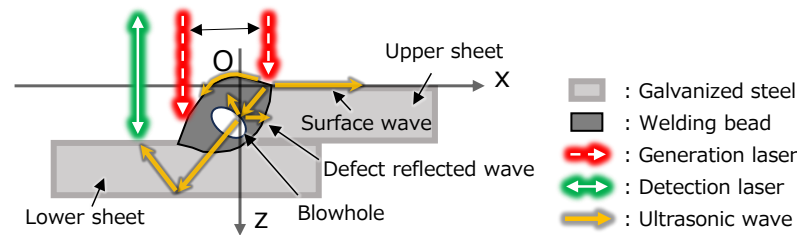


Figure 1. Schematic of the blowhole detection method using laser ultrasonics in the lap joint welding of a galvanized steel sheet.

2.2. Experimental Setup

Figure 2 shows the experimental setup. The specimen was a joint of a 2.3 mm-thick galvanized steel sheet with fillet lap joint welds. RT (radiographic testing) determined the location of the defects in the specimen in advance, as shown in Figure 3. A defect with an approximately 1.5 mm diameter existed at the location indicated as “Defect” in Figure 3. The test specimen was placed on top of the measurement device and the lasers were directed upward. A pulsed YAG laser (Nano L 90–100 from Litron Lasers, Rugby, UK) with a wavelength of 1064 nm, pulse width of 7 to 9 ns, repetition rate of 100 Hz, and pulse energy of 25 mJ was used as the generation laser. A galvanometer mirror system controlled the generating position on the sample surface. The diameter of the generated laser beam at the sample surface was approximately 1 mm. A laser interferometer (Quartet-1500 from Bossa Nova Technologies, Culver City, CA, USA) with a wavelength of 532 nm was used as the detection laser. The irradiation of the generating laser was detected using a photodetector (DET10N/M from THORLABS, Newton, NJ, USA), which was used as the trigger for recording the ultrasonic. One B-scope corresponded to an *xz* cross-section since the generating laser was scanned in the *x* direction. Static measurement of a specific cross-section was without movement in the *y* direction of the weld line. Traveling measurement involved movement in the *y* direction.

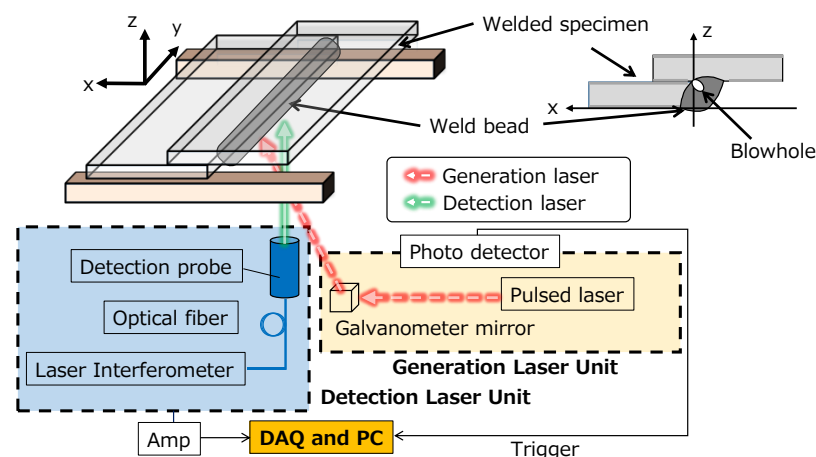


Figure 2. Schematic diagram of the experimental system.

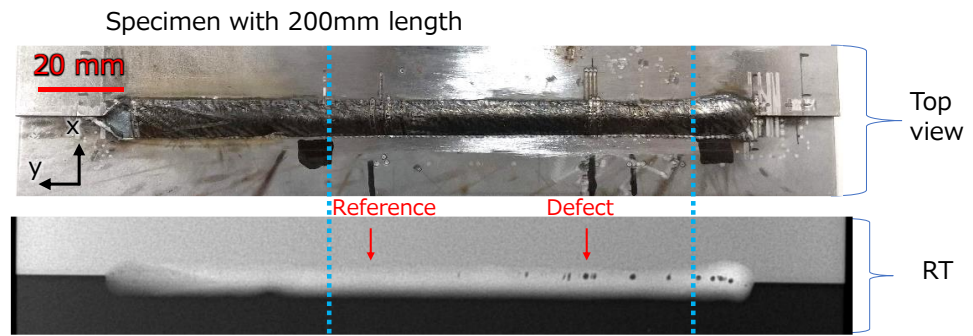


Figure 3. Appearance of the specimen and the RT result.

2.3. Experimental Result

Static measurements were taken under the positional conditions of generation and detection, as shown in Figure 4a. The generation gap Δx was 0.1 mm, and the generation range was set to $-3\sim 3$ mm. As a result, the number of generation points was 61. The measurement result for a defect-free cross-section (“Reference” in Figure 3) is shown in Figure 4b, and that for a defective cross-section (“Defect” in Figure 3) is shown in Figure 4c. The red boxes in the figure include the longitudinal reflected wave on the back surface and conversion from longitudinal to transverse wave. The comparison of the area indicated by the yellow circle shows that attenuation was observed in the presence of defects. This generation and detection points arrangement allows the affected waves transmitted through the defect to arrive after the surface lateral waves and before the Rayleigh waves, making it possible to evaluate the signal attenuation.

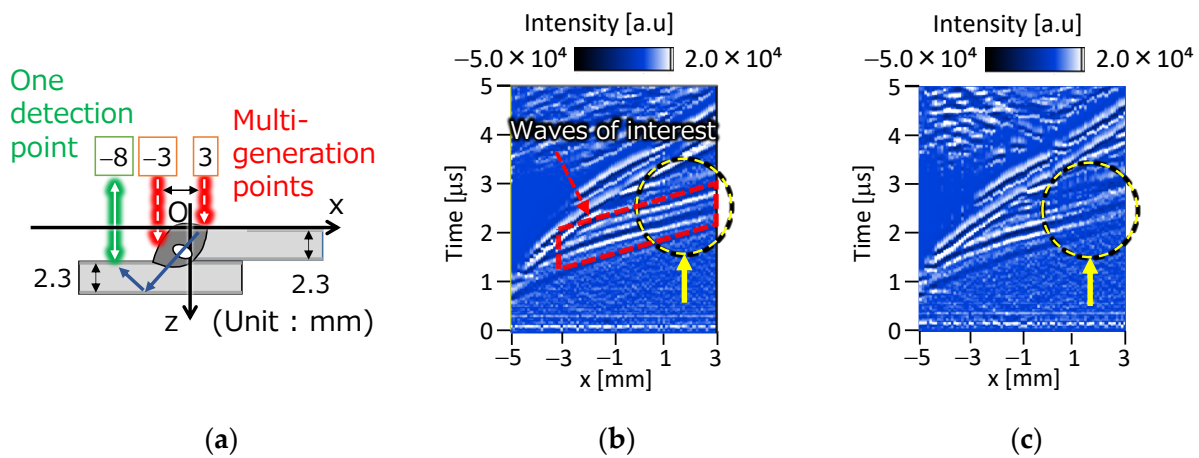


Figure 4. B-scope result for the specimen in Figure 3. (a) Irradiation points of the lasers. (b) Without defect. (c) With defect.

The area containing the focused wave was extracted, and the root mean square (“RMS”) within the extraction area was calculated for each generation position as a measure of signal intensity. Figure 5 shows the RMS distribution. The slope values of those plots were used to determine the presence or absence of a defect in the $x > 0$ region, where the attenuation could be observed. In practice, a slope calculation was performed on the distribution normalized by the RMS distribution obtained for the defect-free section. Therefore, if the slope value was negative, it was judged that attenuation had occurred (i.e., that a defect was present).

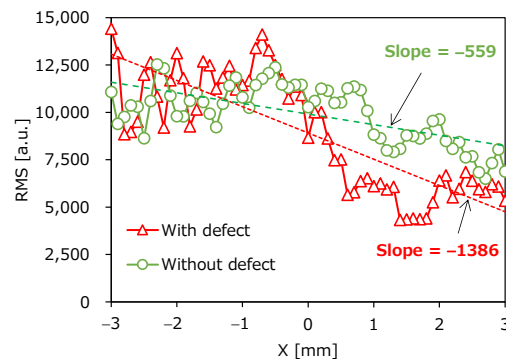


Figure 5. RMS of the extracted signal and its slope at each cross-section with or without defects.

Next, the traveling measurement was performed to measure the cross-section continuously while moving the specimen in the y direction. Continuous inspection for defects while moving in the direction of the weld line is possible because laser ultrasonics is a non-contact measurement. The measurement range was within the dotted line shown in Figure 3. The traveling speed was set to 0.5 m/min, and the generation point gap Δx was increased to 0.5 mm to reduce the number of generation points per cross-section and to improve the spatial resolution in the y direction. With the number of generation points per cross-section reduced to 13, the y -movement distance required to acquire a single B-scope (i.e., the spatial resolution in the y -direction) was determined to be 1.08 mm. Figure 6 shows the correspondence between RT and the defect detection indicator value calculated by applying the previous judgment method to the traveling measurement. It can be seen that there was a correspondence between the portion of the slope value, which is the detection indicator for each cross-section, above a certain value, and the location of the defect in the RT image. On the other hand, it could be observed that the magnitude of the detection indicator for defects varied. The reason for the variation in the detection indicator is that the slope of the underlying signal distribution, in other words, the attenuation, is different. This variation can lead to a difference in the detection of defects depending on the setting of the threshold value.

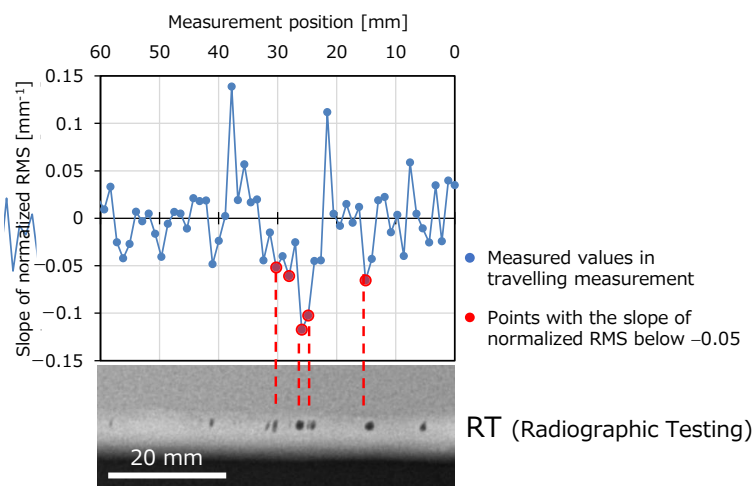


Figure 6. Variation of the normalized RMS slope as a detection indicator in the dynamic measurement range.

Therefore, in the next section, we clarify the reason for the variation in the detection indicator when traveling of the laser ultrasonic method is accompanied, and the relationship between spatial resolution and detection probability with a finite element simulation.

3. Analysis Method

As described in the previous section, the defect detection methods proposed in our previous study resulted in variations in the detection indicators. We first obtained X-ray-CT images of specimens and investigated the relationship between the defects and the detection indicators. As a result, it was found that even when the defect shape was almost the same, the detection indicator varied. Since it is considered that the cause of the variation is not only the defect's shape and position, this study focused on the decrease in spatial resolution during the traveling measurement and examined it through analysis.

This study examined ultrasonic propagation of the ablation mode excited by laser irradiation using FEM analysis [19] with ComWAVE v.11 (ITOCHU Techno-Solutions Corporation, Tokyo, Japan), an ultrasonic analysis software.

Analysis Conditions

The constructed model was a three-dimensional model, as shown in Figure 7. The material parameters of the base material in the analysis were assumed to be steel with a longitudinal wave velocity of 5900 m/s, transverse wave velocity of 3200 m/s, density of 7900 kg/m³, and the defective area as a vacuum. This is because the inner space of a blowhole caused by zinc vapor is almost a vacuum containing only a small amount of hydrogen, and zinc is believed to adhere to the inner wall during the cooling process [20]. Even if zinc vapor or other substances remain in the defect due to insufficient cooling, it is safe to treat the defect as a vacuum because the waves are almost completely reflected from the viewpoint of acoustic impedance.

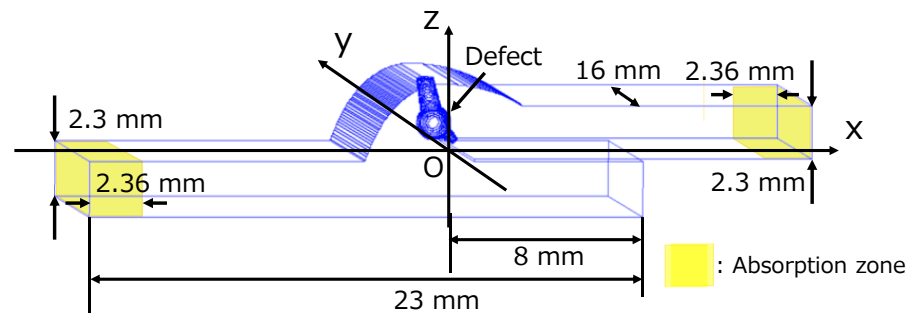


Figure 7. The 3D model of lap joint welding involves a blowhole for FEM analysis.

The pressure wave generated by laser irradiation is known as a one-cycle waveform [21], and the pressure wave used in the analysis was assumed to be a 5 MHz wave representing a propagating wave. The mesh size was 0.05 mm, which is sufficiently small compared to the wavelength of 0.64 mm calculated from the propagation speed of the slowest transverse wave and the frequency of the given ultrasonic.

The base metal existed at both ends of the model in the welding and longitudinal directions, and the propagating waves were not reflected back. Therefore, an absorption zone was established to absorb the propagating waves and minimize reflections from the boundary. The thickness of the absorption band was set to 2.36 mm, twice the thickness of the longest wavelength, with the longitudinal wave of 1.18 mm.

Since many of the defects observed in the X-ray CT of the specimens had similar shapes, a three-dimensional defect model was created based on the X-ray CT results as shown in Figure 8a, combining cones and a sphere, whose external forms are shown in Figure 8b,c.

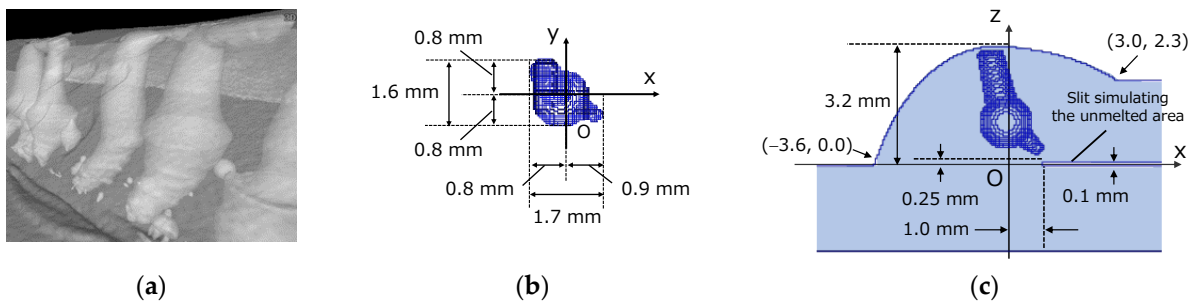


Figure 8. Defect shape in the FEM model and its example of the actual shape. (a) X-ray CT results. (b) Defect shape in the xy cross-section. (c) Defect shape in the xz cross-section.

In this study, we examined a measurement method that was single-point detection and multi-point generation, but not the simultaneous excitation of ultrasonic waves at multiple points. In other words, the experimental conditions shown in Figure 3 resulted in 61 excitation and detection points per cross-section. On the other hand, the software analyzes a single ultrasonic propagation at once. Thus, analysis of one cross-section requires 61 calculations. To obtain more efficient analytical results, we focused on the wave reciprocal theorem, widely known in ultrasonic testing research. The reciprocal theorem states that switching the generation and detection points can obtain the same waveforms. Applying this to the irradiation conditions in this study means that the same waveform is obtained by one generation point and multiple detection points after exchanging the generation and detection positions. This allows us to obtain the B-scope of one cross-section in one calculation. Therefore, the generating and detecting points are exchanged in the subsequent analysis. However, the notation of generation/detection in the figures indicates the original position. As in the experiment, the generating and detecting points in the xz plane were set in the range $x = -8$ mm for the detecting point and $x = -3\sim 3$ mm for the generating point in 0.1 mm gaps, as shown in Figure 9.

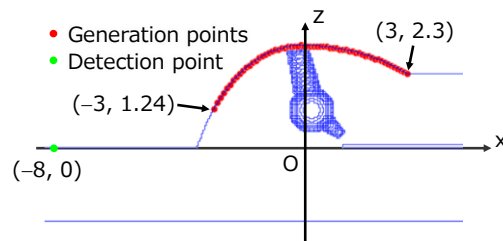


Figure 9. Position of generation and detection in the analysis.

On the other hand, since the defect shape is not uniform in the y direction of the weld line, the detection indicator depends on the irradiation position in the y direction. The analysis range in the y direction was set to $-2.56\sim 2.56$ mm, which includes the region where the defect exists. However, as shown in Figure 10, when the measurement was made while traveling in the y direction, the generation point became oblique in the xy plane, and the obliquity changed, depending on the traveling speed. In the experimental measurement, the laser beams emitted in the order from right to left, as shown in Figure 10, and when they reached the left end of the generation range, they instantly returned to the right end and repeated the same behavior toward the left end, as in the previous case. The detecting point also moved in the y direction, so the reciprocal theorem described earlier was no longer applicable. In addition, even if the defect geometry is the same, the analysis must be redone depending on the measurement conditions such as a traveling speed change.

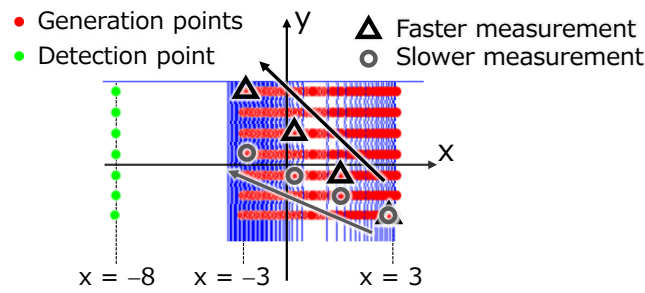


Figure 10. Correspondence between the traveling speed and measurement position.

In this study, we devised a method to evaluate the results of the traveling measurement by picking up data, as shown in Figure 10, from a dataset obtained by repeating the calculation of static measurement at a position shifted by 0.04 mm in the weld line direction, according to the traveling speed. As a result, not only can the reciprocal theorem be used, but evaluation can also be performed simply by changing the pickup location, even if conditions such as the traveling speed change.

4. Result and Discussion

4.1. Data Processing

This section shows how to process the data at each stationary cross-section. The same as in the experiment, one analytical B-scope was obtained from the results of one cross-section. Figure 5 shows the RMS distribution at each generation point. It can be seen that even when there were no defects, there was signal attenuation due to diffusion as the propagation distance increased. In the following, a normalized RMS distribution was used to emphasize attenuation due to defects by dividing the calculated RMS distribution by the defect-free RMS distribution. Figure 11 shows the normalized RMS distributions for the B-scope and the extraction region for the $y = 0$ mm and -0.48 mm cross-section. Although the results differed depending on the y position, the attenuation of the ultrasonic signal was observed similarly as in the experiment. Repeating the same operation for each y position provided a two-dimensional (x, y) normalized RMS value map, as shown in Figure 12. A three-color scale (green-yellow-red) was applied to the map according to the degree of relative RMS value. Points that decreased from the RMS value of the no-defect part were less than 1 (green), and those that increased were higher than 1 (red). This map shows the degree of attenuation of ultrasonic waves generated at each (x, y) point until they reached the detecting point $(-8, y)$. The red boxes indicate the defect locations, and three xz cross-sections through the defects are also shown. Ultrasonic waves generated from the top or right side of the defect were expected to attenuate by the time they reached the detecting position on the left side, and the results vaguely showed this tendency.

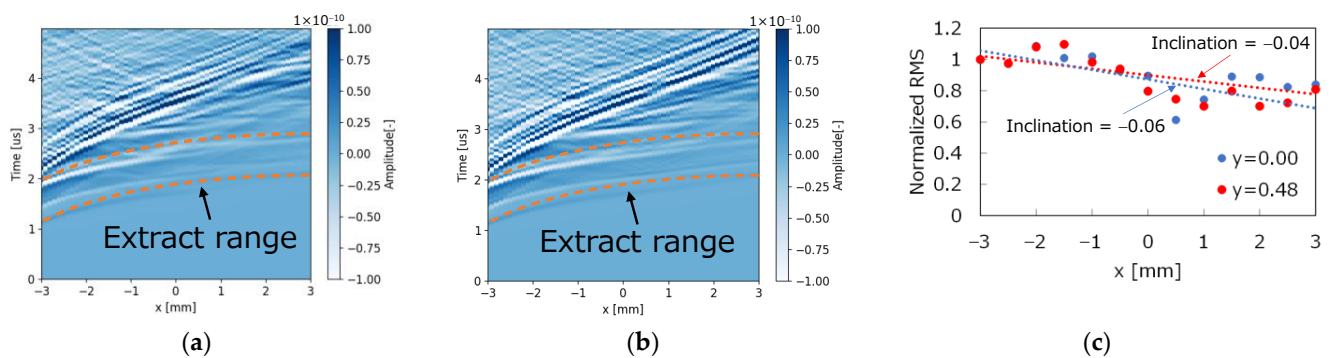


Figure 11. B-scope and RMS distribution at $y = 0$ mm and $y = -0.48$ mm. (a) B-scope, $y = 0$ mm. (b) B-scope, $y = -0.48$ mm. (c) RMS distribution.

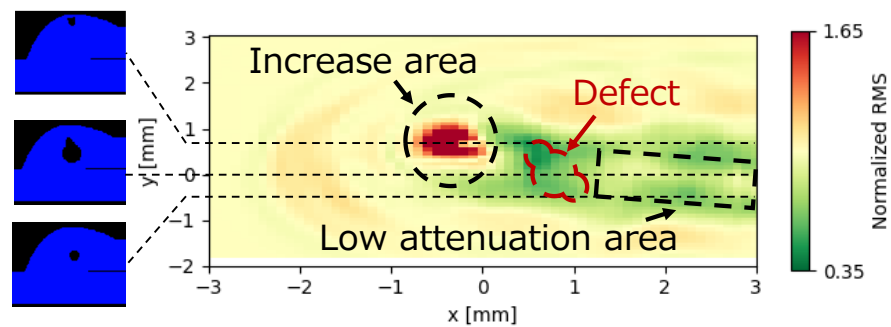


Figure 12. Normalized RMS map with the simulated defect.

However, as shown by the rectangular black dotted line, there was a region of low attenuation, even though the cross-section passed almost through the center of the defect. This is because the ultrasonic waves reached the defect, diffracted on the $+x$ side from the defect, and then re-met on the $-x$ side to strengthen and reduce attenuation.

Furthermore, in areas where defects existed near the surface, the normalized RMS value increased due to reflections from the defects, as shown by the black dotted circular line. The increasing area was on the negative x -axis, meaning on the left side of the figure, which caused the slope of the RMS distribution to be large and negative, as shown in the schematic diagram in Figure 13. This makes determining the defect easier. It was found that this method, which aimed to capture the attenuation, not only captured the attenuation but also a signal increase close to the detecting point when a defective reflected wave was observed.

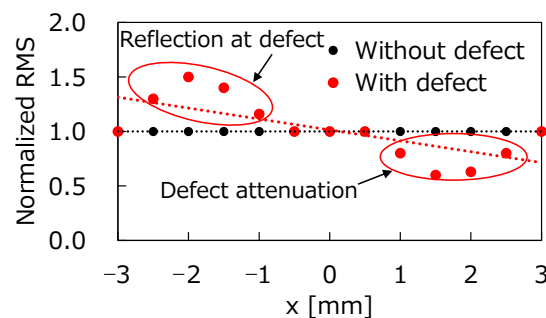


Figure 13. Schematic diagram showing factors of the RMS value increase/decrease due to defects.

4.2. Measurement with Traveling

The data obtained by measurements with traveling were equivalent to acquiring data obliquely on the RMS map. At higher traveling speeds, this oblique angle becomes larger, which is supposed to reduce the probability of passing through the attenuation zone, indicating a defect. The traveling measurement was calculated by selecting data from the results shown in Figure 12. Thirteen points were picked up every 0.5 mm in the x -axis direction according to the experimental conditions for traveling measurements described in Figure 6. When the repetition rate of the laser was 100 Hz and the traveling speed was 0.5 m/min, the distance traveled in the y -axis direction per irradiation resulted in 0.08 mm. Therefore, the B-scope of the 0.5 m/min traveling measurement can be reproduced by picking up the point every 0.5 mm on the x -axis and every 0.08 mm on the y -axis. The cases with 0.25 and 1.0 m/min traveling speeds can be reproduced by picking up the point every 0.04 and 0.16 mm in the y -axis, respectively. An example of a path on the normalized RMS map at each speed is shown in Figure 14.

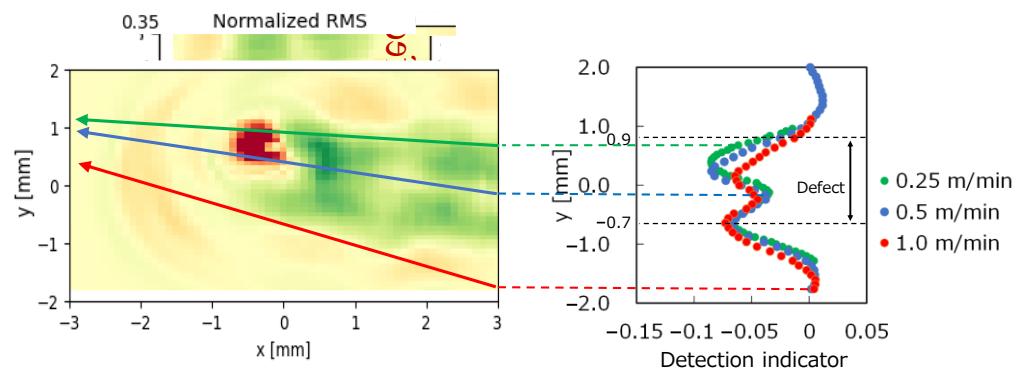


Figure 14. Difference of paths by traveling speed and distribution of largest slope.

The pickup path changes when the start point changes, even at the same traveling speed. A normalized RMS distribution is obtained for each path, and its slope is the detection indicator value for that path. The detection indicator values obtained for each path with a slight shift of the starting point within the analysis range are summarized for 0.25, 0.5, and 1.0 m/min, respectively, as shown in the graph on the right side of Figure 14. The value of the y -axis is set to the starting position of each cross-section during the traveling measurement.

In the case of actual measurement, since one pass irradiation includes 13 points, the following path starts at a point 13 points ahead in the y -axis direction from the start point of the previous path. Figure 15a,b shows the paths when the measurement starts at $y = -1.84$ mm and $y = -1.20$ mm for a traveling speed of 0.5 m/min, and Figure 15c shows the distribution of the detection indicator values calculated for each path. A larger absolute value of the detection indicator means that the defect is more likely to be determined as a defect. In this case, the detection indicator starting the measurement at $y = -1.84$ mm is about twice that at $y = -1.20$ mm. Therefore, even when we measure the same defects at the same traveling speed, the ease of defect identification depends on the starting position of the measurement. Similarly, Figure 16 shows a result for a 0.25 m/min traveling speed. Figure 16 also shows that the ease of defect discrimination varies depending on the measurement start position.

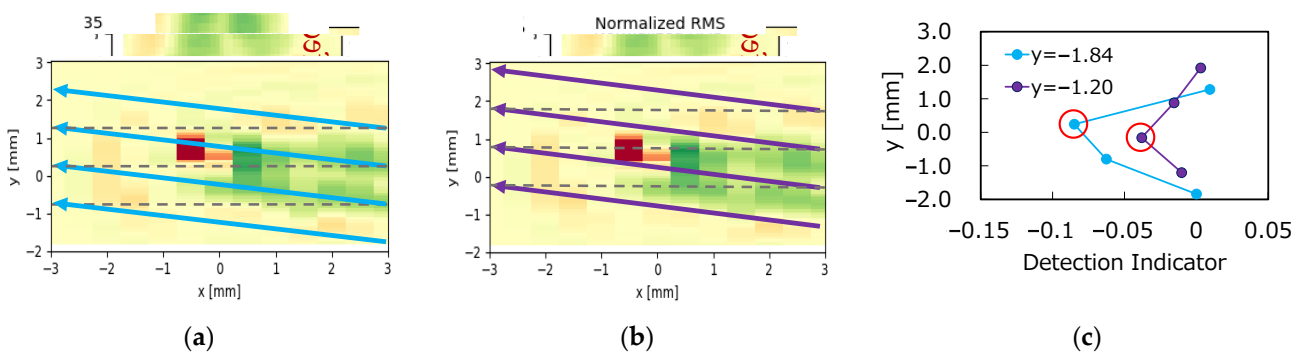


Figure 15. Change in the RMS distribution with a change in measurement position at 0.5 m/min. (a) Starting at $y = -1.84$ mm. (b) Starting at $y = -1.20$ mm. (c) Detection indicator distribution starting at $y = -1.84$ mm, $y = -1.20$ mm.

Once the starting position is determined, the cross-section through the measurement path is also determined. The detection indicator at the cross-section is calculated by picking up the data with equal intervals from the right graph of Figure 14. The interval was 0.54 mm at the traveling speed of 0.25 m/min, 1.08 mm at 0.50 m/min, and 2.16 mm at 1.0 m/min, respectively. The value that had the most significant influence on the judgment of the presence or absence of defects was the value of the largest detection indicator (circled in red in Figure 15c), which also changed depending on the starting position of

the measurement. Therefore, it was found that one of the reasons for the variation in the indicators in our previous proposed defect detection method is the change in the indicators with the difference in the scanning position relative to the defect.

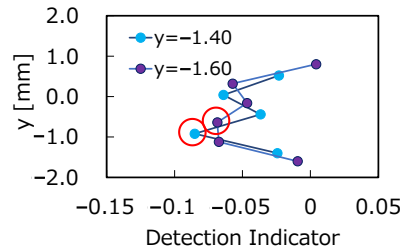


Figure 16. Detection indicator distribution at 0.25 m/min, starting at $y = -1.60$ mm, $y = -1.40$ mm.

4.3. Discussion

As shown in Figure 15c, the maximum absolute value of the detection indicator depends on the starting position of the measurement, even for the same defect. Only the maximum value obtained by each starting position is summarized by traveling speed in Figure 17. When the traveling speed was 0.25 m/min, the distribution was $-0.085 \sim -0.067$, and when the traveling speed was 1.0 m/min, the distribution was $-0.073 \sim -0.014$. The distribution approached zero as the traveling speed increased. Assuming that a defect is judged to be detected when the indicator is less than -0.05 , the detection probability at each traveling speed is as shown in Figure 17, and it was confirmed analytically that the slower the traveling speed, the easier the defect is detected.

Traveling speed (Equivalent repetition rate: 100 Hz)	Detection indicator			Detection probability	Equivalent repetition rate (Traveling speed: 0.5 m/min)
	-0.1	-0.05	0		
0.25 m/min	●●●●●	●●●●●	●●●●●	100 %	200 Hz
0.5 m/min	●●●●●	●●●●●	●●●●●	60 %	100 Hz
1.0 m/min	●●●●●	●●●●●	●●●●●	55 %	50 Hz

Figure 17. Distribution of the largest slope at each traveling speed. The color of the dots corresponds to the color coding of the traveling speed in Figure 14.

On the other hand, there are different ways to increase the detection probability beside the lower traveling speed such as increasing the laser repetition rate. When considering the traveling speed of 0.5 m/min in the middle of Figure 17 as a standard, halving the traveling speed to 0.25 m/min is equivalent to doubling the laser repetition rate to 200 Hz (refer to the equivalent repetition rate in the right-most column of Figure 17). If the traveling speed is 0.5 m/min with a threshold value of -0.05 , it is predicted that a repetition rate of 200 Hz is sufficient for stable detection. Therefore, the required repetition rate of the generating laser can be determined from the required detection accuracy and threshold setting.

When traveling measurements were conducted on the same defect, the value of the detection indicator varied depending on the starting position of the measurement. Therefore, it was found that defect sizing is difficult based on the proposed indicator values. A different detection method needs to be developed for sizing and localization. However, the application of UT is originally difficult for thin sheets such as those used in this study, and it will be challenging to propose a new method.

5. Conclusions

In our previous report, we experimentally developed a detection method using laser ultrasonics for blowholes that occur in the lap joint welding of galvanized steel sheets. This method was based on the attenuation of ultrasonic waves passing through a defect, but its detection indicator values varied. This study aimed to analytically elucidate the reason for this variation in detection indicator values and clarify the relationship between spatial

resolution and detection probability. We proposed and established an analytical method to efficiently reproduce the traveling measurement results by creating a lap joint welded sheet model that includes the defect geometry.

We found that one of the reasons for the variation in the defect detection indicator value with traveling by the laser ultrasonic method is the variation in the detection indicator value depending on the scanning position. In addition, it was possible to propose the performance required for the ultrasonic exciting side such as the traveling speed and the required repetition frequency of the generation laser by back-calculating the spatial resolution from the rate of detection needed.

Author Contributions: Conceptualization, methodology, experiments, N.O. and K.N.; Writing—original draft preparation, N.O.; Writing—review and editing, K.N.; Resources, supervision, funding acquisition, K.N., T.S., K.K., S.N., T.E. and S.A. All authors have read and agreed to the published version of the manuscript.

Funding: This research received no external funding.

Data Availability Statement: The data presented in this study are available on request from the corresponding author. The data are not publicly available due to the samples being sensitive and the need for specialist processing of the data.

Acknowledgments: The authors would like to thank Pony Industry Co., Ltd. (Osaka, Japan) for the technical support and advice with the X-ray CT measurements.

Conflicts of Interest: The authors declare no conflict of interest.

References

1. Toyoda, M. Brittle Fracture Strength and Fracture Toughness Evaluation of Welds. *J. Jpn. Weld. Soc.* **1993**, *62*, 603–616. [[CrossRef](#)]
2. Matsui, H. Arc Welding of Galvanized Steel Sheets. *J. Jpn. Weld. Soc.* **1997**, *66*, 423–427. [[CrossRef](#)]
3. Kato, K. The Most Up-to-Date Radiographic Examination Technology. *J. Jpn. Weld. Soc.* **2001**, *70*, 646–649. [[CrossRef](#)]
4. Jen, C.-K.; Cao, B.; Nguyen, K.T.; Loong, C.A.; Legoux, J.-G. On-Line Ultrasonic Monitoring of a Die-Casting Process Using Buffer Rods. *Ultrasonics* **1997**, *35*, 335–344. [[CrossRef](#)]
5. Hernandez-Valle, F.; Dixon, S. Initial Tests for Designing a High Temperature EMAT with Pulsed Electromagnet. *NDT E Int.* **2010**, *43*, 171–175. [[CrossRef](#)]
6. Gan, T.H.; Hutchins, D.A. Air-Coupled Ultrasonic Tomographic Imaging of High-Temperature Flames. *IEEE Trans. Ultrason. Ferroelectr. Freq. Control* **2003**, *50*, 1214–1218. [[CrossRef](#)] [[PubMed](#)]
7. Drain, L.E. *Laser Ultrasonics Techniques and Applications*, 1st ed.; Routledge: Oxfordshire, UK, 2019.
8. Ochiai, M.; Butsuen, T.; Miura, T.; Kuroda, H.; Soramoto, S.; Kanemoto, S. Sizing of Micro Cracks Using Laser-induced Broad-band Surface Waves. *J. Nucl. Sci. Technol.* **2001**, *43*, 275–281. [[CrossRef](#)]
9. Yamamoto, S.; Hoshi, T.; Miura, T.; Semboshi, J.; Ochiai, M.; Fujita, Y.; Ogawa, T.; Asai, S. Defect Detection in Thick Weld Structure Using Welding In-Process Laser Ultrasonic Testing System. *Mater. Trans.* **2014**, *55*, 998–1002. [[CrossRef](#)]
10. Tanaka, T.; Izawa, Y. Noncontact Detection of Internal Defects in Carbon Steel by Laser Ultrasonics. *Rev. Laser Eng.* **2002**, *30*, 140–145. [[CrossRef](#)]
11. Bustamante, L.; Jeyapakash, N.; Yang, C.-H. Hybrid Laser and Air-Coupled Ultrasonic Defect Detection of Aluminium and CFRP Plates by Means of Lamb Mode. *Results Phys.* **2020**, *19*, 103438. [[CrossRef](#)]
12. Zeng, W.; Ming Cai, F.; Wang, F.; Miao, L.; You, F.; Yao, F. Finite Element Simulation of Laser-Generated Ultrasonic Waves for Quantitative Detection of Internal Defects in Welds. *Optik* **2020**, *221*, 165361. [[CrossRef](#)]
13. Jon, S.; So, J.; He, N.; Sok, K.; Choe, L.; Kim, K.; So, S. An Application of Optical Fiber Fizeau Interferometer to the Detection of Internal and Surface Defects in Metal. *Chem. Phys. Lett.* **2019**, *725*, 8–13. [[CrossRef](#)]
14. Hong, S.-C.; Abetew, A.-D.; Lee, J.-R.; Ihn, J.-B. Three Dimensional Evaluation of Aluminum Plates with Wall-Thinning by Full-Field Pulse-Echo Laser Ultrasound. *Opt. Lasers Eng.* **2017**, *99*, 58–65. [[CrossRef](#)]
15. Li, Y.; Hou, S.; Chai, Y.; Zhou, Y.; Zou, Y. Nondestructive Measurement of the Grain Size of Laser Cladding Coatings Using a Laser Ultrasonic Method. *Appl. Opt. AO* **2022**, *61*, 1885–1891. [[CrossRef](#)] [[PubMed](#)]
16. Garcin, T.; Schmitt, J.H.; Militzer, M. In-Situ Laser Ultrasonic Grain Size Measurement in Superalloy INCONEL 718. *J. Alloys Compd.* **2016**, *670*, 329–336. [[CrossRef](#)]
17. Nomura, K.; Matsuida, T.; Kadota, K.; Era, T.; Asai, S. Study on Blowhole Detection in Fillet Welded Sheet of Lap Joint by Laser Ultrasonic Technique. *Q. J. Jpn. Weld. Soc.* **2023**, *41*, 141–149. [[CrossRef](#)]
18. Kadota, K.; Matsuida, T.; Nomura, K.; Era, T.; Asai, S. In-Line Detection of Internal Defects for Lap Joint Welding of Galvanized Steel Sheet by Laser Ultrasonic Technique. In Proceedings of the IIW International Conference on Welding and Joining, Tokyo, Japan, 17–18 July 2022; pp. 192–195.

19. Ikegami, Y.; Sakai, Y.; Nakamura, H. A Highly Accurate Ultrasonic Simulator Capable of Over One Billion Elements for Non-Destructive Evaluations. *e-J. Nondestruct. Test.* **2010**, *15*, 177–190.
20. Otani, T. Arc Weldability of Zinc Coated Steel Sheets. *Weld. Int.* **1999**, *13*, 527–535. [[CrossRef](#)]
21. Murray, T.W.; Wagner, J.W. Laser Generation of Acoustic Waves in the Ablative Regime. *J. Appl. Phys.* **1999**, *85*, 2031–2040. [[CrossRef](#)]

Disclaimer/Publisher’s Note: The statements, opinions and data contained in all publications are solely those of the individual author(s) and contributor(s) and not of MDPI and/or the editor(s). MDPI and/or the editor(s) disclaim responsibility for any injury to people or property resulting from any ideas, methods, instructions or products referred to in the content.